Electronic Supplementary Information (ESI) for

Hydrogen bonding bolstered head-to-tail ligation of functional chromophores in 0D SbF_3·Glycine adduct for short-wave ultraviolet nonlinear optical material

Zhiyong Bai, Jihyun Lee, Chun-Li Hu,* Guohong Zou,* and Kang Min Ok*

Department of Chemistry, Sogang University, Seoul, 04107, Republic of Korea

E-mail: kmok@sogang.ac.kr

Experimental Procedures

Synthesis. Glycine (Alfa Aesar, 98+%) and SbF_3 (Alfa Aesar, 98%) were used as starting reagents. Typically, stoichiometric glycine (10 mmol, 0.75 g) and SbF_3 (10 mmol, 1.79g) were dissolved in 10 mL deionized water under constant stirring at 40 ℃ until a clear solution was prepared. The solution was filtered and then evaporated at room temperature. After about three days, small block crystals were harvested. Powder X-ray diffraction (XRD) pattern of the ground bulk crystals is in good agreement with the simulation pattern (Figure S1).

Powder X-ray diffraction. The test was executed at room temperature on a Rigaku MiniFlex 600 diffractometer equipped with Cu Kα radiation (λ = 1.5406 Å). The 2θ range was 10−60° with a scan step width of 0.02° and a fixed counting time of 5 s per step.

Single-crystal structure determination. The single crystal X-ray diffraction data were collected on a Bruker APEX-II CCD diffractometer utilizing Mo Kα radiation (λ = 0.71073 Å) at 273.15 K. Data reduction, cell refinement, and absorption corrections were conducted with the program APEX 4. The structure was solved by intrinsic phasing method and refined on F^2 by full-matrix least-squares techniques using the program Olex2[1]. The structure was checked by program PLATON[2] and no higher symmetry was found. Crystal data and structure refinement are given in Table S1. Atomic coordinates with equivalent isotropic displacement parameters, bond lengths, bond angels, torsion angels, and hydrogen bonds are presented in Table S2-S6.

UV-Vis reflectance spectrum. Ultraviolet−visible (UV−vis) transmittance spectra were collected on a JASCO V-660 spectrometer in the wavelength range of 200−800 nm. In order to determine the band gap, the diffuse reflectance spectral data were subsequently transferred to the function of reflectance by using Kubelka function:

$$F(R) = \frac{(1-R)^2}{2R} = \frac{K}{S}$$

where *R* denotes the reflectance, *K* the absorption coefficient and S the scattering factor. In the *F(R)* versus *E* (eV) plot, extrapolating the linear part of the rising curve to zero provides the onset of the absorption.

SHG Response. According to method proposed by Kurtz and Perry[3], powder SHG measurements were carried out by using 1064 nm coherent light, generated by Q-switched Nd: YAG laser, as incident source. Specifically, polycrystalline samples of title compound and KH_2PO_4 (KDP) were ground and sieved into distinct particle size ranges (<20, 20-45, 45-63, 63-75, 75-90, 90-125, 125-150, 150-200, and 200-250 μm). Sieved KDP powder was used as a reference. The intensity of the frequency-doubled output emitted from the sample was collected using a photomultiplier tube.

TGA test. Thermogravimetric analysis (TGA) was performed by using a SCINCO TGA-n 1000 thermal analyzer. Powder samples in weight of about 6 mg were loaded to alumina crucibles and heated from 25 to 600 °C at a rate of 10 °C min^{-1} under flowing air.

Computation Method. The electronic structures and optical properties were performed using a plane-wave basis set and pseudo-potentials within density functional theory (DFT) implemented in the total-energy code CASTEP.[4] For the exchange and correlation function, Perdew-Burke-Ernzerhof in the generalized gradient approximation was chosen.[5] The interactions between the ionic cores and the electrons were described by the norm-conserving pseudopotential.[6] The following valence-electron configurations were considered in the computation: Sb-$5s^25p^3$, F-$2s^22p^5$, C-$2s^22p^2$, N-$2s^22p^3$, O-$2s^22p^4$, and H-$1s^1$. The number of plane waves included in the basis sets was determined by a cutoff energy of 850 eV. The numerical integration of the Brillouin zone was performed using a Monkhorst-Pack k-point sampling of 5 × 5 × 5. The other parameters and convergent criteria were the default values of the CASTEP code.

The calculation of second-order NLO properties were based on length-gauge formalism within the independent-particle approximation.[7] We adopted the Chen's static formula, which has been derived by Rashkeev et al. and later modified by Chen's group.[6, 8] The static second-order NLO susceptibility can be expressed as

$$\chi^{\alpha\beta\gamma} = \chi^{\alpha\beta\gamma}(\mathrm{VE}) + \chi^{\alpha\beta\gamma}(\mathrm{VH}) + \chi^{\alpha\beta\gamma}(\text{two bands})$$

where $\chi^{\alpha\beta\gamma}$(VE) and $\chi^{\alpha\beta\gamma}$(VH) give the contributions to $\chi^{\alpha\beta\gamma}$ from virtual-electron processes and virtual-hole processes, respectively; $\chi^{\alpha\beta\gamma}$(two bands) is the contribution to $\chi^{\alpha\beta\gamma}$ from the two-band processes.

References

[1] O. V. Dolomanov, L. J. Bourhis, R. J. Gildea, J. A. K. Howard, H. Puschmann, *J. Appl. Crystallogr.* **2009**, *42*, 339-341.

[2] S. A. L., *J. Appl. Crystallogr.* **2003**, *36*, 7-13.

[3] S. K. Kurtz, T. T. Perry, *J. Appl. Phys.* **1968**, *39*, 3798-3813.

[4] a) V. W. Milman, B.; White, J. A.; Pickard, C. J.; Payne, M. C.; Akhmatskaya, E. V.; Nobes, R. H., *Int. J. Quantum Chem.* **2000**, *77*, 895−910; b) M. D. L. Segall, P. J.; Probert, M. A.; Pickard, C. J.; Hasnip, P. J.; Clark, S. J.; & Payne, M. C., *J. Phys.: Condens. Matter* **2002**, *14*, 2717−2744.

[5] J. P. B. Perdew, K.; Ernzerhof, M. P, *Phys. Rev. Lett.* **1996**, *77*, 3865−3868.

[6] J. L. Lin, M. H.; Liu, Z. P.; Chen, C.; Pickard, C. J., *Phys. Rev. B* **1999**, *60*, 13380−13389.

[7] C. Aversa, J. E. Sipe, *Phys. Rev. B Condens. Matter* **1995**, *52*, 14636-14645.

[8] S. N. L. Rashkeev, W. R.; Segall, B., *Phys. Rev. B* **1998**, *57*, 3905-3919.

Table S1. Crystal data and structure refinement for $SbF_3 \cdot Gly$.

Empirical formula	$C_2H_5F_3NO_2Sb$
Formula weight	253.82
Temperature [K]	273.15
Crystal system	monoclinic
Space group (number)	*Pc* (7)
a [Å]	6.9889(4)
b [Å]	6.7515(4)
c [Å]	6.4707(4)
β [°]	90.289(2)
Volume [Å^3]	305.32(3)
Z	2
ρ_{calc} [gcm^{-3}]	2.761
μ [mm^{-1}]	4.510
F(000)	236
Radiation	Mo K_α (λ=0.71073 Å)
2θ range [°]	6.03 to 55.01 (0.77 Å)
Index ranges	$-9 \leq h \leq 9$ $-8 \leq k \leq 8$ $-8 \leq l \leq 8$
Reflections collected	6264
Independent reflections	1366 R_{int} = 0.0508 R_{sigma} = 0.0381
Data / Restraints / Parameters	1366/2/84
Goodness-of-fit on F^2	1.087
Final *R* indexes [$I \geq 2\sigma(I)$] Final *R* indexes [all data]	R_1 = 0.0202 wR_2 = 0.0476 R_1 = 0.0206 wR_2 = 0.0479
Largest peak/hole [eÅ^{-3}]	0.73/-0.71
Flack *x* parameter	0.20(4)

Table S2. Atomic coordinates and U_{eq} [Å^2] for SbF_3·Gly. U_{eq} is defined as 1/3 of the trace of the orthogonalized U_{ij} tensor.

Atom	***x***	***y***	***z***	U_{eq}
Sb1	0.67092(6)	0.28163(4)	0.67117(6)	0.01907(13)
F1	0.9467(6)	0.2318(5)	0.7599(7)	0.0298(9)
F2	0.7867(5)	0.5156(6)	0.5609(5)	0.0374(8)
F3	0.7527(5)	0.1105(6)	0.4464(5)	0.0336(8)
O1	0.3138(6)	0.0960(8)	0.4687(7)	0.0356(10)
O2	0.4679(6)	0.3807(6)	0.4223(7)	0.0312(9)
C1	0.2039(9)	0.3184(10)	0.2074(12)	0.0295(16)
C2	0.3347(10)	0.2539(9)	0.3825(11)	0.0232(12)
N1	0.0552(6)	0.1666(8)	0.1633(7)	0.0228(9)
H1A	0.142391	0.442301	0.243949	0.035
H1B	0.279208	0.340860	0.084107	0.035
H1C	-0.012458	0.202723	0.052735	0.027
H1D	-0.022075	0.155520	0.271577	0.027
H1E	0.111268	0.050515	0.139251	0.027

Table S3. Anisotropic displacement parameters [Å^2] for SbF_3·Gly. The anisotropic displacement factor exponent takes the form: $-2\pi^2[\, h^2(a^*)^2U_{11} + k^2(b^*)^2U_{22} + \ldots + 2hka^*b^*U_{12}\,]$

Atom	U_{11}	U_{22}	U_{33}	U_{23}	U_{13}	U_{12}
Sb1	0.01816(17)	0.01898(18)	0.02004(17)	0.0001(3)	−0.00260(11)	0.0001(3)
O1	0.0303(19)	0.040(3)	0.036(2)	0.014(2)	−0.0131(16)	−0.008(2)
F2	0.0366(18)	0.0296(19)	0.046(2)	0.0153(17)	−0.0176(15)	−0.0150(15)
F3	0.0298(16)	0.039(2)	0.0318(16)	−0.0114(16)	0.0013(13)	0.0052(15)
O2	0.0248(18)	0.030(2)	0.038(2)	0.0021(19)	−0.0157(15)	−0.0039(18)
C2	0.018(3)	0.030(3)	0.022(3)	−0.002(2)	−0.005(3)	0.001(2)
F1	0.019(2)	0.036(2)	0.034(2)	0.0021(15)	−0.0078(17)	0.0033(13)
C1	0.018(4)	0.028(3)	0.042(5)	0.008(3)	−0.012(3)	−0.007(2)
N1	0.019(2)	0.025(2)	0.024(2)	0.000(2)	−0.0063(18)	−0.004(2)

Table S4. Bond lengths and angles for SbF_3·Gly.

Atom–Atom	Length [Å]	Atom–Atom–Atom	Angle [°]	Atom–Atom–Atom	Angle [°]
Sb1–F2	1.914(3)	F2–Sb1–F3	94.86(16)	N1–C1–C2	111.3(5)
Sb1–F3	1.946(3)	F2–Sb1–O2	75.72(15)	N1–C1–H1A	109.4
Sb1–O2	2.243(4)	F2–Sb1–F1	80.79(15)	N1–C1–H1B	109.4
Sb1–F1	2.036(4)	F3–Sb1–O2	80.06(16)	C1–N1–H1C	109.5
O1–C2	1.213(9)	F3–Sb1–F1	80.30(16)	C1–N1–H1D	109.5
O2–C2	1.290(8)	F1–Sb1–O2	147.79(18)	C1–N1–H1E	109.5
C2–C1	1.516(9)	C2–O2–Sb1	113.5(4)	H1C–N1–H1D	109.5
C1–H1A	0.9700	O1–C2–O2	125.5(6)	H1C–N1–H1E	109.5
C1–H1B	0.9700	O1–C2–C1	121.5(6)	H1D–N1–H1E	109.5
C1–N1	1.486(7)	O2–C2–C1	113.0(6)		
N1–H1C	0.8900	C2–C1–H1A	109.4		
N1–H1D	0.8900	C2–C1–H1B	109.4		
N1–H1E	0.8900	H1A–C1–H1B	108.0		

Table S5. Torsion angles for $SbF_3 \cdot Gly$.

Atom–Atom–Atom–Atom	**Torsion Angle [°]**
Sb1–O2–C2–O1	0.9(10)
Sb1–O2–C2–C1	−177.4(5)
O1–C2–C1–N1	0.4(10)
O2–C2–C1–N1	178.7(6)

Table S6. Hydrogen bonds of $SbF_3 \cdot Gly$.

D–H···A [Å]	[ARU]	d(D–H) [Å]	d(H···A) [Å]	d(D···A) [Å]	<(DHA) [°]
N1–H1C···F1	[1454.01]	0.89	1.92	2.750(7)	154
N1–H1D···F3	[1455.01]	0.89	1.97	2.830(6)	163
N1–H1C···F2	[2464.01]	0.89	2.36	2.924(6)	121
N1–H1E···F1	[2454.01]	0.89	2.36	2.865(6)	116
N1–H1E···O1	[2554.01]	0.89	2.05	2.832(7)	145

Translation of ARU-Code to CIF and Equivalent Position Code: [2564.] = [2_564] = x, 1-y, -1/2+z; [2554.] = [2_554] = x, -y, -1/2+z; [1454.] = [1_454] = -1+x, y, -1+z; [1455.] = [1_455] = -1+x, y, z; [2454.] = [2_454] = -1+x, -y, -1/2+z.

Table S7. Bond valence sum (BVS) calculations for SbF_3·Gly.

Bond	**Distance/Å**	**BVS**
Sb1-F2	1.9140	0.920
Sb1-F3	1.9460	1.763
Sb1-F1	2.0360	2.424
Sb1-O2	2.2430	**2.906**

Table S8. The calculated dipole moments of [$SbOF_3$] polyhedra in SbF_3·Gly (Units: Debye).

Species	***x*-component**	***y*-component**	***z*-component**	**Magnitude**
[$Sb1OF_3$]	5.23	-1.65	-6.82	8.76
[$Sb1OF_3$]$^{\#1}$	5.23	1.65	-6.82	8.76
Sum	10.46	0	-13.64	

Table S9. The calculated SHG coefficient d_{ij} for SbF_3·Gly.

d_{ij} (pm/V)	Magnitude
d_{11}	-0.380
$d_{12} = d_{26}$	-0.495
$d_{13} = d_{35}$	-1.438
$d_{15} = d_{31}$	-0.926
$d_{24} = d_{32}$	**1.475**
d_{33}	-1.176
d_{eff}	1.538
Powder SHG efficiency (200-250 μm)	3.6 × KDP[a]

[a] The d_{36} of standard KDP is 0.39 pm/V. The largest tensor d_{32} and d_{eff} of SbF_3·Gly is *ca.* 3.8 and 3.9 times that of d_{36} of KDP, respectively, consistent with the experimental results.

For point group *m*, there are 10 nonvanishing SHG tensor:

$$\begin{pmatrix} d_{11} & d_{12} & d_{13} & 0 & d_{15} & 0 \\ 0 & 0 & 0 & d_{24} & 0 & d_{26} \\ d_{31} & d_{32} & d_{33} & 0 & d_{35} & 0 \end{pmatrix}$$

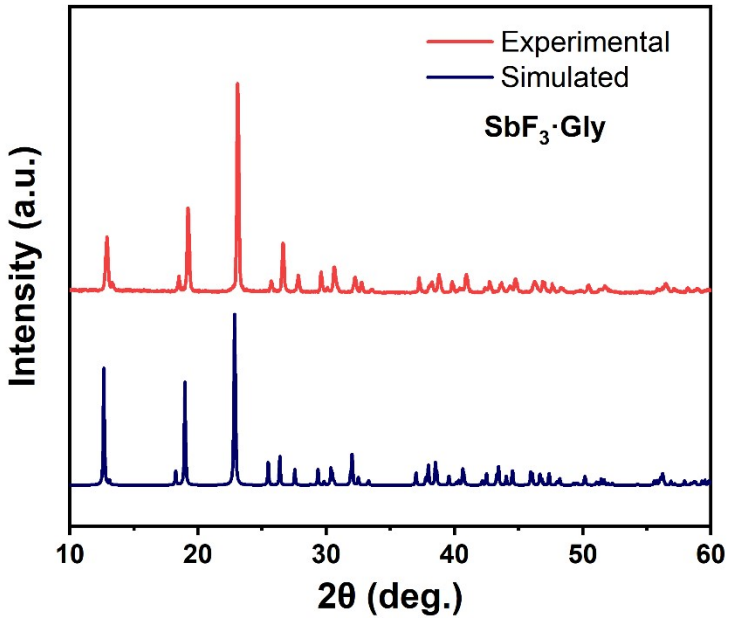

Fig. S1 The powder X-ray diffraction (PXRD) patterns for SbF_3·Gly.

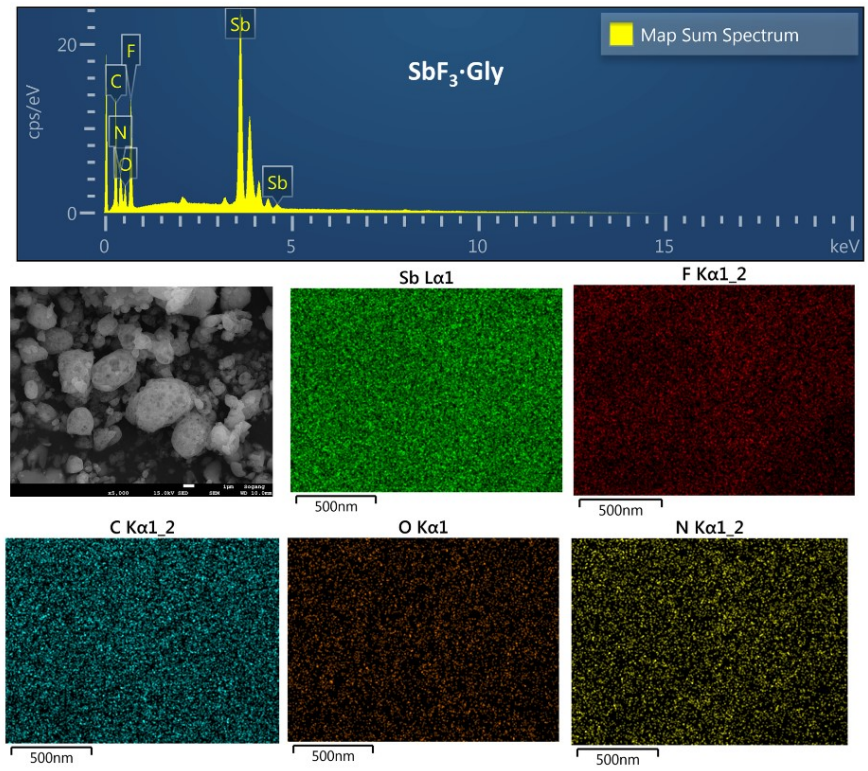

Fig. S2 The EDS mapping for SbF_3·Gly.

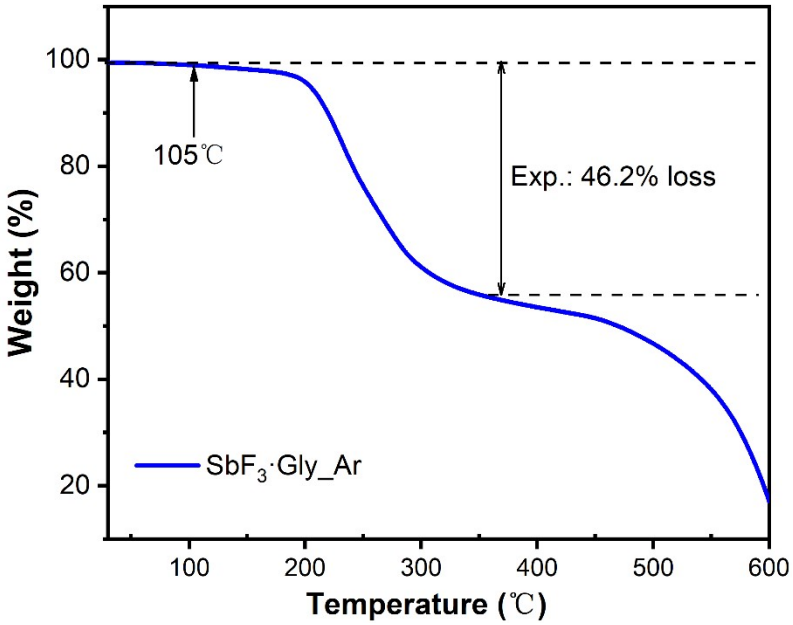

Fig. S3 The thermogravimetric (TG) plot of SbF_3·Gly recorded from 30 to 600 ℃. It can be stable up to *ca.* 105 ℃ and above this temperature it starts a slow decomposition. The obvious weight loss started from about 200 ℃ and the decomposition process is complicated.

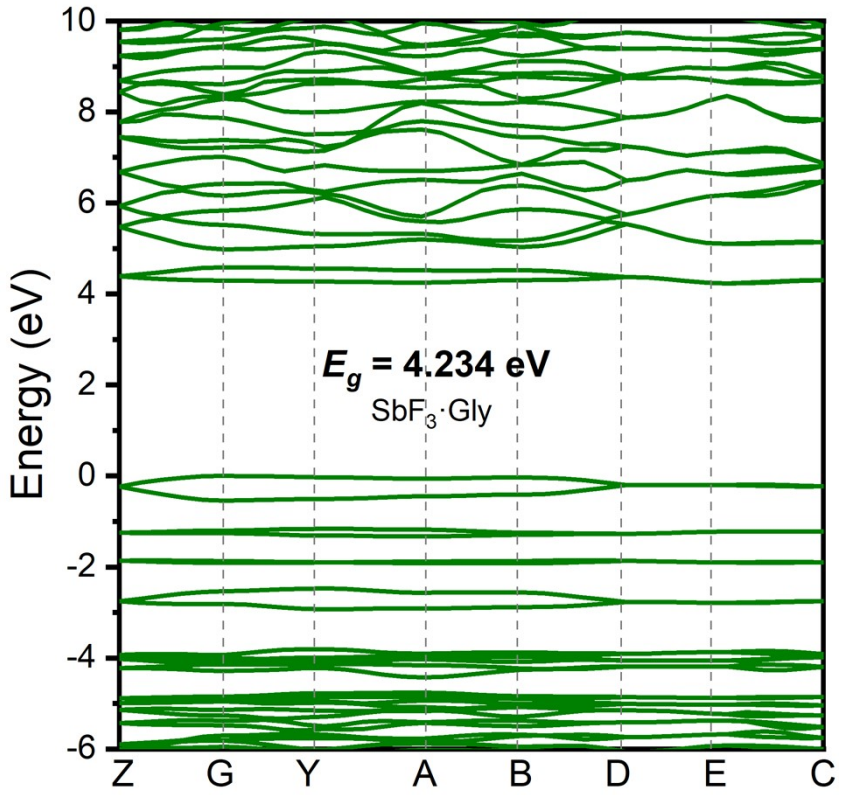

Fig. S4 The calculated band structure for SbF_3·Gly.

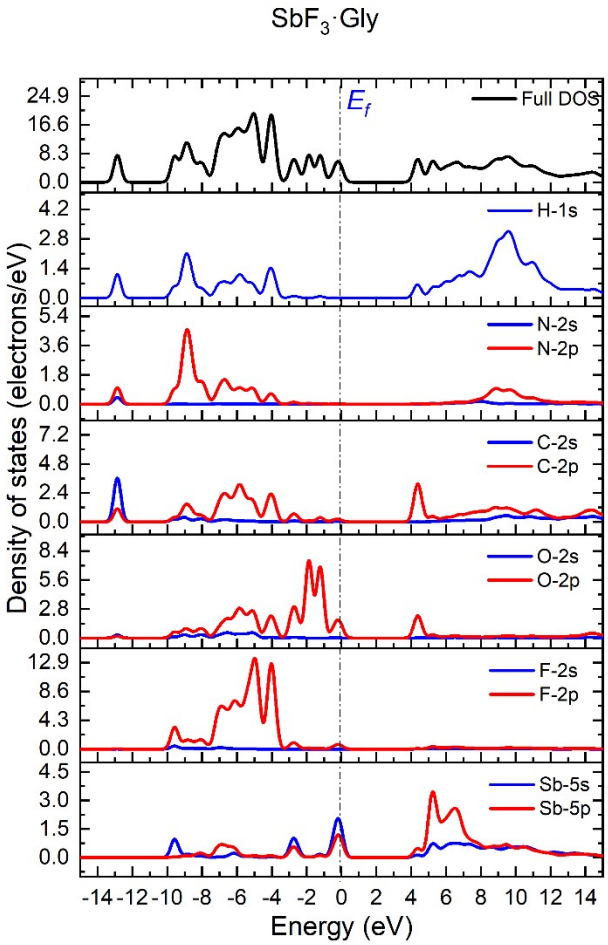

Fig. S5 The calculated partial densities of states (PDOS) for SbF_3·Gly.

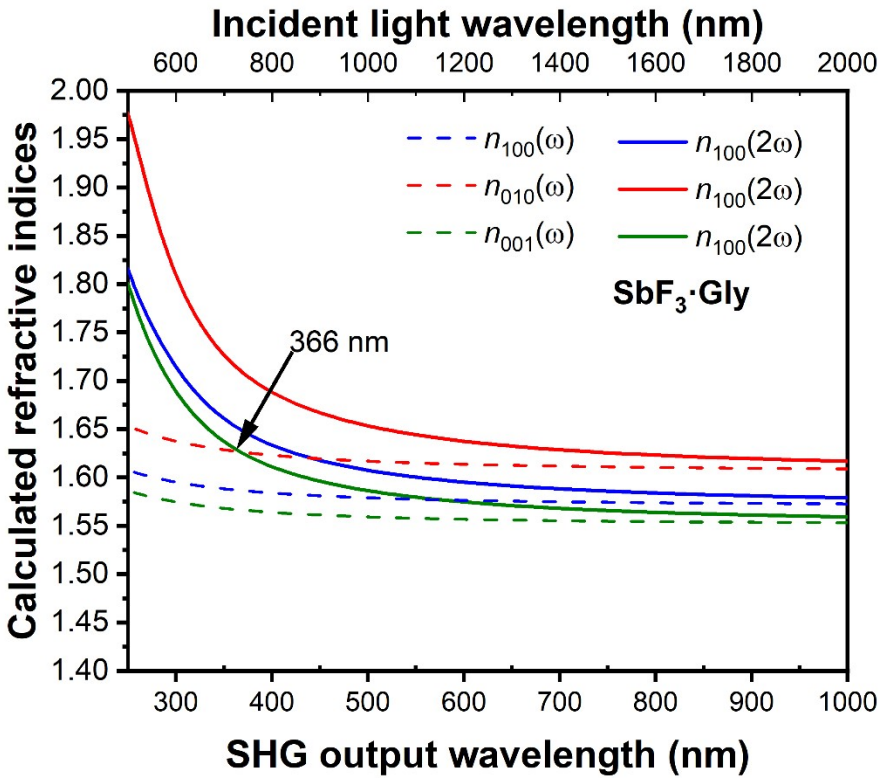

Fig. S6 The evaluated phase-matching (PM) ability of SbF_3·Gly based on the calculated refractive indices.